NASA MEMO 5-14-59E

NASA

MEMORANDUM

EXPERIMENTAL ALTITUDE PERFORMANCE OF JP-4 FUEL AND LIQUID-OXYGEN ROCKET ENGINE WITH AN AREA RATIO OF 48

By Anthony Fortini, Charles D. Hendrix, and Vearl N. Huff

Lewis Research Center
Cleveland, Ohio

NATIONAL AERONAUTICS AND SPACE ADMINISTRATION
WASHINGTON
May 1959

NATIONAL AERONAUTICS AND SPACE ADMINISTRATION

MEMORANDUM 5-14-59E

EXPERIMENTAL ALTITUDE PERFORMANCE OF JP-4 FUEL AND LIQUID-OXYGEN ROCKET ENGINE WITH AN AREA RATIO OF 48

By Anthony Fortini, Charles D. Hendrix, and Vearl N. Huff

SUMMARY

The performance for four altitudes (sea-level, 51,000, 65,000, and 70,000 ft) of a rocket engine having a nozzle area ratio of 48.39 and using JP-4 fuel and liquid oxygen as a propellant was evaluated experimentally by use of a 1000-pound-thrust engine operating at a chamber pressure of 600 pounds per square inch absolute. The altitude environment was obtained by a rocket-ejector system which utilized the rocket exhaust gases as the pumping fluid of the ejector. Also, an engine having a nozzle area ratio of 5.49 designed for sea level was tested at sea-level conditions.

The following table lists values from faired experimental curves at an oxidant-fuel ratio of 2.3 for various approximate altitudes:

	Sea-level engine		Large-area-ratio engine				
	Sea level	Corrected to vacuum	Sea level	51,000 Ft	65,000 Ft	70,000 Ft	Corrected to vacuum
Characteristic velocity, c*, ft/sec	5520	5520	5520	5520	5520	5520	5520
Specific impulse, I, lb-sec/lb	250	273	223	289	298	303	311
Thrust coefficient, C_F	1.46	1.60	1.31	1.69	1.74	1.77	1.82

Specific impulse from sea level to computed vacuum conditions for a nozzle with an area ratio of 48.39 increased by 39.5 percent, whereas the specific impulse of the sea-level engine (area ratio of 5.49) increased by 9.2 percent.

Specific impulse for the large-area-ratio engine was 10.8 percent lower than for the small-area-ratio engine for sea-level conditions. At vacuum conditions the specific impulse of the large-area-ratio engine was 13.9 percent higher than for the sea-level engine.

For the large-area-ratio engine, the gas flow in the nozzle separated at an area ratio of 16. The separation pressure was 0.3 of the sea-level pressure.

The average heat-transfer rate at an oxidant-fuel ratio of 2.30 for the additional surface area required by the large-area-ratio nozzle was 0.4 Btu per second per square inch without flow separation. The heat load required by the additional surface was 33 percent of the total heat load.

INTRODUCTION

At each altitude the optimum performance level of a rocket engine is obtained by the nozzle that gives complete expansion. Therefore, the missile or airplane designer who uses a fixed nozzle over a range of altitude is faced with the selection of a design point and the prediction of engine performance at off-design operation. The objective of this investigation was to measure the performance of a large-area-ratio engine at various altitudes and to compare the performance of the large-area-ratio engine with an engine designed for sea level. To fulfill these objectives, a prototype ejector for simulation of altitude was designed, built, and tested at the Lewis laboratory (during the year 1954). A literature survey showed many types of ejector geometries and their respective performance. Ejector performance data reported in the literature vary depending upon the geometry and the ejector application. For example, data for an ejector with a convergent primary nozzle and with cylindrical ejector tubes are given in references 1 and 2.

The prototype ejector differed from that of references 1 and 2 in that high primary pressures and a convergent-divergent nozzle were used. The information gained from the prototype was applied to a rocket system in which the rocket acted as the primary nozzle, which in turn evacuated its own atmosphere. The performance of the rocket was then measured at four altitudes and is reported herein.

Researchers have studied overexpansion (nozzle exit pressure lower than ambient pressure) in rocket nozzles for the purpose of determining performance at off-design conditions. For example, performance data for red fuming nitric acid and aniline at various expansion ratios can be found in reference 3. These data apply to a limited expansion range,

which was obtained by varying the chamber pressure and holding back pressure constant, whereas the data presented in this report were obtained by varying the back pressure and holding the chamber pressure constant.

The tests to be described in this report were made with a 1000-pound-thrust engine which had a chamber pressure of 600 pounds per square inch absolute and utilized the propellant JP-4 fuel and liquid oxygen. The large-area-ratio engine consisted of a sea-level engine to which was welded a water-cooled nozzle extension. The rocket was instrumented for thrust and other performance parameters. The nozzle extension was instrumented for heat rejection. Exploratory tests were made for internal wall pressure of the nozzle extension in order to determine the point of flow separation, the separation pressure, and the nozzle exit pressure when the nozzle flowed full. The exploratory tests are not reported herein, but separation pressure, exit pressure, and the point of separation are given.

SYMBOLS

A	nozzle flow cross-sectional area
C_F	thrust coefficient
c^*	characteristic velocity, ft/sec
F	thrust, lb
f	fuel mass flow rate, lb/sec
g	gravitational constant, 32.17 ft/sec^2
I	specific impulse, lb-sec/lb
L^*	characteristic length, in.
o	oxidant mass flow rate, lb/sec
P	total pressure, lb/sq in. abs
p	static pressure, lb/sq in. abs
p_m	mean effective pressure acting on nozzle wall after flow separation, lb/sq in. abs
q	heat-transfer rate, Btu/(sec)(sq in.)

W total propellant mass flow rate, lb/sec

ϵ area ratio, A_e/A_t

η percent of theoretical performance

Subscripts:

b barometric

c combustion chamber

e nozzle exit or engine

fr frozen composition

n nozzle extension

o ambient

s separation point

t throat

v vacuum

DESCRIPTION OF EQUIPMENT AND PROCEDURE

The equipment to be described permits testing a rocket engine under both sea-level and simulated altitude conditions for either fixed or variable chamber pressure. The entire rocket engine was enclosed in a capsule, and an ejector system utilizing the contained rocket was used to pump the capsule pressure to the desired value. Figure 1 shows the ejector assembly.

Equipment

Engine. - The engine was rated at 1000-pound thrust with a nominal chamber pressure of 600 pounds per square inch absolute. The characteristic length of the combustion chamber was 30 inches, the combustion chamber contraction ratio was 3.83, the nominal sea-level nozzle area ratio was 5.25, and the nozzle had a 15° half-angle. The engine was cooled by water flowing through hydrostatically formed helical cooling

passages as shown in figure 2. Nickel was used for the inner walls and Inconel for the outer walls. The internal engine surface area was calculated to be 80 square inches. Two models were made to these specifications.

Nozzle extension. - A conical nozzle extension was welded to one of the sea-level engines (engine section) of figure 2; a photograph of the welded assembly is shown in figure 3. The over-all area ratio of the engine section with the extension was 48.39. The nozzle extension had a 15° half-angle and was water cooled. The cooling water for the extension was separate from that for the engine to facilitate measurements of over-all heat transfer in the extension. The nozzle-extension internal surface area was calculated to be 196.4 square inches.

Injector. - The propellants were injected into the combustion chamber by means of a removable injector made up of a nickel face with a stainless steel body (fig. 4). The design concept employed a large number of like-on-like impingement units to provide fine atomization, uniform propellant distribution, and thorough coverage across the flat injector face. The injector contained 82 units of like-on-like impinging doublets for fuel and 70 for oxidant. These units were arranged in alternate rows for fuel and oxidant, as indicated in figure 4 and provided parallel finely atomized sheets of fuel and oxidant. Two holes in each fuel unit, 0.020 inch in diameter, were tried. Because of the way the fuel flowed through the internal manifold, the momentum of one impinging stream from each fuel unit was found to be greater for the holes nearest the fuel inlet. To equalize the momentum the opposite hole of each fuel unit was drilled to a 0.025-inch diameter.

Propellants. - The propellants used were liquid oxygen and JP-4 fuel. The liquid oxygen was stated by specification to be 99.5 percent pure. The fuel was taken from the laboratory supply.

Ejector tube and capsule. - The rocket engine was totally enclosed within the capsule as shown schematically in figure 1. Variation in nozzle pressure ratio was obtained by a change in ejector tube diameter. Each diameter resulted in a specific pressure altitude for a fixed chamber pressure and oxidant-fuel ratio. The high-velocity exhaust gas of the rocket under test served as the primary jet of the ejector. The primary jet flowed into an 8-foot-long pipe with a diameter of either 9 or $9\frac{5}{8}$ inches. A simple water bath was sufficient to prevent warpage and burnout of the ejector tubes.

The capsule contained not only the rocket engine but also the instrument for measuring thrust. One static-pressure tap at each end of the capsule was used for measuring capsule pressure. The capsule static-pressure lines were carried up through the capsule cover so that liquids would not be trapped in the manometer lines. The cover was attached to the bedplate by quick-disconnect clamps. The flexure-plate thrust stand, propellant lines, coolant lines, and thrust-load-cell support were attached to the bedplate.

Instrumentation. - Propellant and coolant flow rates were determined by rotating-vane type flowmeters. Thrust was measured by a strain-gage transducer. Chamber pressure was measured by two strain-gage pressure transducers and by a direct-writing Bourdon tube recorder. Coolant water temperatures were measured separately for the engine section and the nozzle extension by iron-constantan thermocouples which had an ice-bath cold junction. Oxidant temperature was measured by a copper-constantan thermocouple which had a liquid-nitrogen cold junction. With this temperature and data from reference 4 the density of the oxidant was obtained. The density of the fuel was measured before each set of runs by use of a hydrometer. Capsule pressures were recorded by mercury manometers which were photographed continually at a rate of 2 frames a second.

Calibrations were made before every set of runs for thrust, chamber pressure, and temperatures. The fuel flowmeters and coolant flowmeters were calibrated with water, whereas the oxidant meters were calibrated with liquid oxygen. Over-all instrument accuracy (from the pickup to the reduced data) for each instrument during the calibrations was ± 0.5 percent of full scale.

Test facilities. - The engine and the thrust-measuring load cell were enclosed within the capsule, as shown in figure 1. The load cell, which was hermetically sealed, was found to be sensitive to environmental pressure and was therefore calibrated for pressure effects within the capsule and with the normal preload due to propellant lines. A maximum correction of 2.7 percent was applied to the thrust reading for sensitivity of the load cell to environmental pressure.

Propellant flow rates were controlled by pressurization of the tanks, with nitrogen gas on the fuel and helium gas on the oxidizer. The line from the oxidant tank to the engine contained a coil immersed in a tank of liquid nitrogen. This coil was used to cool the oxygen to liquid-nitrogen temperature before metering. The oxidant flowmeters, located after the coil, were also immersed in the same tank of liquid nitrogen. The oxidant temperature was measured directly after the flowmeters.

Nitrogen gas purges were used in the capsule and in both propellant flow lines. Ignition was accomplished at low propellant flow. After high flow was established, the capsule purge was stopped. The shutdown sequence involved stopping propellant flows and starting all purges. All firing operations were remotely controlled. Electrical controls provided for immediate shutdown of the engine operation in the event of a burnout, low coolant flow, no ignition, faulty chamber pressure, or flameout. Such controls were required for the prevention of explosions within the capsule and safe operation of the test cell.

Procedure

Before each set of runs for a day's operation the thrust stand was calibrated by applying an external force to the engine mount with the capsule in place and the engine ready to operate. The propellant tanks were pressurized to give a constant chamber pressure and the desired oxidant-fuel ratio. Sea-level runs of the large- and small-area-ratio engines were made with the capsule in place but without an ejector tube. For the simulated altitude runs of the large-area-ratio engine, an ejector tube was attached to the capsule. Because of the time response of the manometers, altitude runs were made for a time duration of approximately 20 seconds.

PRECISION

Careful consideration and a large expenditure of effort were given to calibrations and analysis of recorded output of the instruments. The precision of the data could be checked by two methods. The first was the reproducibility of calibrations, and the second was agreement between dual recordings of the same measured quantity during a run. The following table gives estimates of precision:

Measurement	Estimated precision, percent	Method
Propellant flow	±3/4	Dual meters
Coolant flow	±1	Calibration reproducibility
Chamber pressure	±1	Dual meters
Thrust	±1	Calibration
Coolant temperature change	±10	Fluctuation of outlet temperature on run trace
Oxidant density	±1/2	Calibration of thermocouple

RESULTS

Experimental data are listed in table I. Part (a) of table I contains the experimental data for sea-level operation of a sea-level engine and a large-area-ratio engine; part (b) contains experimental data for the large-area-ratio engine at simulated altitude.

Performance curves for the sea-level engine are shown in figures 5 and 6 for sea-level and computed vacuum operation, respectively. Characteristic velocity c^*, specific impulse I, thrust coefficient C_F, and engine heat-transfer rate q_e are plotted against oxidant-fuel ratio o/f. Theoretical curves for a fixed area ratio based on equilibrium and frozen expansion obtained from references 5 and 6 are also presented.

Figures 7, 8, and 9 present the experimental performance of the large-area-ratio engine at sea level, at various altitudes, and at computed vacuum operation, respectively. Values of c^*, I, C_F, q_e, and q_n are again plotted against the parameter o/f. Also presented in figure 9 are the theoretical performance curves for the fixed large-area-ratio engine. The theoretical curves were obtained from references 5 and 6.

Figure 10 shows the percent of theoretical vacuum specific impulse against o/f for each experimental point for which the nozzle was flowing full.

Performance is summarized in the following table for the large- and small-area-ratio engines operating at an o/f of 2.30 and various approximate altitudes. The performance values were obtained from faired curves of figures 5 to 9.

	Small-area-ratio engine		Large-area-ratio engine				
	Sea level	Corrected to vacuum	Sea level	51,000 Ft	65,000 Ft	70,000 Ft	Corrected to vacuum
Characteristic velocity, c^*, ft/sec	5520	5520	5520	5520	5520	5520	5520
Specific impulse, I, lb-sec/lb	250	273	223	289	298	303	311
Thrust coefficient, C_F	1.46	1.60	1.31	1.69	1.74	1.77	1.82
Heat-transfer rate, q_e, Btu/(sec)(sq in.)	2.20	----	2.10	1.90	1.90	1.90	----
Heat-transfer rate, q_n, Btu/(sec)(sq in.)	----	----	1.05	.40	.40	.40	----

The specific impulse for the large- and small-area-ratio engines from this summary table is presented in figure 11.

DISCUSSION

Throughout the tests reported herein characteristic length L^*, chamber pressure, and injector type were held constant. Three injectors of the same type were used, and the test results indicated no shift in performance. The experimental scatter of the data for figures 5 through 9 from the faired curves was within ±2 percent for c^*, I, and C_F, but the heat-transfer data for the engine and the nozzle extension show a scatter of ±10 percent. All the experimental data fall within the allowable percent error calculated from the individual measurements.

Theoretical Performance

The theoretical curves of figures 5, 6, and 9 were obtained from the results of references 5 and 6. Since the theoretical results of references 5 and 6 are for nozzles with complete expansion, the results for specific impulse and thrust coefficient were corrected for the force resulting from the difference between nozzle exit pressure and ambient pressure acting over the fixed nozzle exit area. For vacuum conditions the ambient pressure was set equal to zero. For sea-level conditions the ambient pressure was set equal to 14.7 pounds per square inch absolute.

Small-Area-Ratio Engine

Sea-level performance. - At maximum specific impulse, which occurs at an o/f of 2.20 (fig. 5), the faired experimental curve of c^* is 93.2 percent of theoretical equilibrium expansion and 95.3 percent of theoretical frozen expansion, whereas the faired curve of I is 88.7 percent of equilibrium and 91.9 percent of frozen. The faired curve of C_F at maximum I is 95.4 percent of equilibrium and 96.7 percent of frozen. The average heat-transfer rate of the engine was found to rise with an increase in o/f to a value of 3.0 Btu per second per square inch at an o/f of 3.0. At the maximum experimental I the heat-transfer rate is 2.1 Btu per second per square inch.

Vacuum performance. - The vacuum performance of the sea-level engine as presented in figure 6 was obtained from the experimental points of figure 5 but with the pressure force (ambient pressure times exit area) added to the measured thrust. The experimental curve of I_V has a maximum which is essentially the same percent of theoretical performance with equilibrium or frozen expansion as for sea-level operation.

Large-Area-Ratio Engine

At sea-level operation the gas flow was visually observed to be separated well within the large-area-ratio nozzle. Therefore, exploratory tests were made to determine the point of flow separation. When the flow was separated at sea-level conditions, the flow-separation area ratio was 16, and at that point the ratio of separation pressure to ambient pressure was 0.3, in agreement with reference 7. The exploratory tests also showed that the exit pressure when the nozzle was flowing full was 0.9 pound per square inch absolute.

Sea-level performance. - The results of figure 7 indicate that, for sea-level operation with flow separation in the nozzle, values of I and C_F are lower than those for the small-area-ratio engine. However, separation results in much higher performance than if the nozzle gases were overexpanded at sea-level conditions (see fig. 11).

The average heat-transfer rate for the engine section and nozzle extension are also presented in figure 7. Both heat-transfer rates increase with o/f but not at the same rate. The heat-transfer rate (within experimental error) for the engine up to an area ratio of 5.49 was the same regardless of whether or not the nozzle extension was present. At an o/f of 2.30, the average heat-transfer rate for the engine section was 2.2 Btu per second per square inch; for the nozzle extension the heat-transfer rate was 1.1 Btu per second per square inch. The heat-transfer area for the engine section was calculated to be 80 square inches, and the nozzle-extension surface up to the point of separation was calculated to be 50 square inches based on a flow-separation area ratio of 16. The remaining portion of the nozzle extension was excluded from the heat-transfer surface area, although admittedly the remaining portion of the nozzle must have sensed some radiant energy. Therefore, the results of figure 7 for the nozzle extension are conservative.

Computing the heat flux to the engine section and nozzle extension by use of the heat-transfer data in table I(a) and the respective surface areas shows that the heat flux to the nozzle with flow separation was approximately 21 percent of the total heat flux (heat flux of engine section plus nozzle extension) and the percentage is insensitive to o/f.

Altitude performance. - An increase in experimental performance for the large-area-ratio engine occurs with an increase in altitude for the three altitudes presented in figure 8. The altitudes listed in figure 8 are average values, for it was noted that the ambient pressure for a fixed ejector configuration varied depending upon the chamber pressure and the o/f. The ambient pressure for each data point is listed in table I(b). Also, table I(b) shows two altitudes for the same rocket

and ejector geometry. A possible explanation for attaining two pressure altitudes with the same ejector tube is that the capsule had small leaks.

The engine-section and nozzle-extension average heat-transfer rates are presented in figure 8 for the nozzle flowing full. This condition results in a heat-transfer surface area of 196.4 square inches for the nozzle extension. At an o/f of 2.30, the heat-transfer rate for the nozzle extension is 0.4 Btu per second per square inch. This amounts to 33 percent of the total heat rejected to the engine plus the extension. The total heat rejected when the nozzle is flowing full is greater than when flow separation is encountered. But the average heat-transfer rate for the nozzle flowing full is much lower than when flow separation occurs because of the difference in heat-transfer surface area.

The data of figures 7 and 8 may be differenced to approximate the heat transferred to the nozzle between area ratios of 16 and 48.39. Computation shows that at an o/f of 2.30 an average heat-transfer rate of approximately 0.16 Btu per second per square inch existed over the aforementioned section of the nozzle, which amounts to 10 percent of the total heat when the nozzle is flowing full.

Vacuum performance. - The vacuum performance of figure 9 for the large-area-ratio engine was obtained from the data points of figure 8, which were corrected to vacuum conditions in the same manner as those for the small-area-ratio engine. A comparison of percent of theoretical performance for vacuum conditions of the large- and small-area-ratio engines is presented in the following table at an o/f of 2.30:

	Small-area-ratio engine		Large-area-ratio engine	
	Percent of theoretical		Percent of theoretical	
	Equilibrium expansion	Frozen expansion	Equilibrium expansion	Frozen expansion
Characteristic velocity, c*	93	96	93	96
Vacuum specific impulse, I_v	88	92	88	93
Vacuum thrust coefficient, $C_{F,v}$	96	97	95	98

With the table and taking into consideration the fairing of the data, there seems to be no change in the percent of theoretical performance between the large- and small-area-ratio engines.

Nature of Expansion Process

Comparison of the experimental C_F curve with the theoretical curve for frozen expansion in figures 5, 6, and 9 indicates the expansion process to be more like frozen than equilibrium. The results of figure 10 show that the actual specific impulse is more nearly a constant percentage of frozen theoretical than of equilibrium theoretical. However, the expansion process is related to the injector, the propellant combination, and the physical size of the nozzle, as well as other factors. Also, the theoretical data were not corrected for three-dimensional effects when compared with the experimental data. Hence, an inference that the real expansion process is either frozen or equilibrium can be drawn only after considerations of factors in addition to those reported herein.

Performance Comparison of Large- and Small-Area-Ratio Engines

The experimental performance of the large- and small-area-ratio engines at an o/f of 2.30 for varying ambient back pressure presented in figure 11 was obtained from figures 5 to 9. The specific impulse for the small-area-ratio engine increased from 250 at sea level to 273 at vacuum conditions, an increase in performance of 9.2 percent. The large-area-ratio engine had an increase in performance from 223 at sea level to 311 at vacuum, an increase of 39.5 percent. At sea-level conditions the large-area-ratio engine produced 10.8 percent less impulse than the sea-level-area-ratio engine; at vacuum conditions the large-area-ratio engine produced 13.9 percent more impulse than the sea-level engine. Figure 11 also shows that the large-area-ratio engine did not produce the large loss in specific impulse from overexpansion, but that flow separation was encountered and resulted in a much higher value of specific impulse for sea-level operation. At sea level, the specific impulse for the overexpanded nozzle was computed to be 112 pound-seconds per pound. The gain in specific impulse was the direct result of increasing the pressure forces acting upon the internal surface of the nozzle exposed to ambient pressure by flow separation. The flow separation effectively varied the nozzle area ratio from 48 to 16.

The faired curves of figure 11 for the small-area-ratio engine were determined from the experimental impulse at sea level and a correction of impulse for back-pressure effects at the various ambient pressures. The overexpansion curve of the large-area-ratio engine was determined by correcting the vacuum specific impulse for the back-pressure effects. The faired curve of the large-area-ratio engine was determined in two sections, the first being a faired curve through the experimental data to the point of incipient flow separation at the nozzle exit. The

ambient pressure at incipient separation was determined by obtaining the nozzle wall exit pressure and assuming that the measured flow-separation pressure ratio at sea level remained constant for various ambient pressures; also, the assumption was made that the nozzle wall exit pressure and the separation pressure were equal for the incipient condition. The second portion of the faired curve was determined by obtaining the nozzle wall pressures at various area-ratio stations and using the following equation:

$$I = \eta I_s + \frac{c^* p_o}{g P_c}\left[\epsilon_s\left(\frac{p_s}{p_o} - 1\right) - \left(1 - \frac{p_m}{p_o}\right)(\epsilon - \epsilon_s)\right]$$

For frozen composition the equation becomes

$$I = 0.925\ I_{s,fr} + \frac{c^* p_o}{g P_c}\left[\epsilon_s\left(\frac{p_s}{p_o} - 1\right) - \left(1 - \frac{p_m}{p_o}\right)(\epsilon - \epsilon_s)\right]$$

The coefficient 0.925 was determined from previous results showing that the performance for theoretical frozen composition does not change with area ratio for a given o/f of 2.30. The mean effective pressure p_m acting on the nozzle wall after the point of separation was assumed to be 0.95 of the ambient pressure p_o, and the separation pressure ratio p_s/p_o was assumed to be 0.30 for all altitudes. For the fixed o/f of 2.30, c^* was 5520 feet per second, P_c was 600 pounds per square inch absolute, and ϵ was 48.39; hence, the above equation reduced to

$$I = 0.925\ I_{s,fr} + 0.2857\ p_o(-0.65\ \epsilon_s - 2.42)$$

By choosing values of p_s, the area ratio at separation ϵ_s was determined from the experimental plot of nozzle wall pressure against area ratio. The ambient pressure for the chosen separation pressure was computed from the constant separation pressure ratio of 0.30. The theoretical specific impulse $I_{s,fr}$ was obtained by calculating P_c/p_s and using reference 5.

Figure 11 shows that the large-area-ratio engine has both higher and lower specific impulse than the small-area-ratio engine depending upon the ambient pressure. Before deriving conclusions from figure 11, the time required to traverse the atmosphere should be considered. For example, if the time spent traversing the lower atmosphere is short relative to the burning time beyond the atmosphere (ambient pressure is essentially zero), it would be advantageous to employ a large-area-ratio engine because of the gain in performance at high altitudes.

CONCLUDING REMARKS

The experimental altitude performance was measured for a JP-4 fuel and liquid-oxygen rocket engine operating at a chamber pressure of 600 pounds per square inch absolute. Experimental performance of an engine with an area ratio of 48.39 was compared with that of an engine having an area ratio of 5.49. The altitude environment was simulated by an ejector system. The following results were obtained:

1. Measured specific impulse at an altitude of 70,000 feet was 303 pound-seconds per pound for the large-area-ratio engine; whereas, the specific impulse was 272 pound-seconds per pound at the same altitude for the small-area-ratio engine. The experimental data corrected to vacuum conditions showed the specific impulse to be 311 and 273 pound-seconds per pound for the large- and small-area-ratio engines, respectively.

2. If it were physically possible for a 48:1 area-ratio nozzle to flow full at sea level, the resulting specific impulse would be lower than if the nozzle encountered flow separation. Flow separation increased the pressure on the internal surface of the nozzle exposed to the ambient pressure by the separation of flow. The increase in pressure resulted in higher performance than for an overexpanded nozzle. Measured specific impulse at sea level was 223 pound-seconds per pound for the large-area-ratio nozzle with the nozzle flow separated. A computed value of specific impulse for the same nozzle flowing full at sea level was 112 pound-seconds per pound.

3. The sea-level performance of the nozzle with flow separation was lower than for the engine designed for sea level (small area ratio); however, poorer performance existed only for a short range of altitude. The measured specific impulse of the sea-level engine and the large-area-ratio engine at sea level was 250 and 223 pound-seconds per pound, respectively.

4. The missile or airplane designer would be cognizant of the additional weight and the cooling requirement for large-area-ratio nozzles. The additional-heat-load requirement with flow separation occurring at an area ratio of about 16 was 21 percent of the total heat load. With the nozzle flowing full (area ratio of 48) the added heat load was 33 percent of the total heat load.

The nozzle extension increased the small area ratio (5.49) of the sea-level engine to 48.39. The average heat-transfer rate for the nozzle extension flowing full was measured to be 0.4 Btu per second per square inch at an oxidant-fuel ratio of 2.3.

5. The ejector system provides a tool for obtaining experimental altitude performance of rocket engines.

Lewis Research Center
National Aeronautics and Space Administration
Cleveland, Ohio, February 18, 1959

REFERENCES

1. Kochendorfer, Fred D., and Russo, Morris D.: Performance Characteristics of Aircraft Cooling Ejectors Having Short Cylindrical Shrouds. NACA RM E51E01, 1951.

2. Kochendorfer, Fred D.: Effect of Properties of Primary Fluid on Performance of Cylindrical Shroud Ejectors. NACA RM E53L24a, 1954.

3. Foster, Charles R., and Cowles, Frederick B.: Experimental Study of Gas-Flow Separation in Overexpanded Exhaust Nozzles for Rocket Motors. PR 4-103, Jet Prop. Lab., C.I.T., May 9, 1949. (Contract W-04-200-ORD-455.)

4. Anon.: Physical Properties and Thermodynamic Functions of Fuels, Oxidizers, and Products of Combustion. Pt. II - Oxidizers. Rep. R-129, The Rand Corp., Feb. 1949.

5. Huff, Vearl N., and Fortini, Anthony: Theoretical Performance of JP-4 Fuel and Liquid Oxygen as a Rocket Propellant. I - Frozen Composition. NACA RM E56A27, 1956.

6. Huff, Vearl N., Fortini, Anthony, and Gordon, Sanford: Theoretical Performance of JP-4 Fuel and Liquid Oxygen as a Rocket Propellant. II - Equilibrium Composition. NACA RM E56D23, 1956.

7. Green, Leon, Jr.: Flow Separation in Rocket Nozzles. Jour. Am. Rocket Soc., vol. 23, no. 1, Jan.-Feb. 1953, pp. 34-35.

8. Minzner, R. A., Ripley, W. S., and Condron, T. P.: U. S. Extension to the ICAO Standard Atmosphere - Tables and Data to 300 Standard Geopotential Kilometers. U. S. Govt. Printing Office, 1958.

TABLE I. - EXPERIMENTAL ROCKET ENGINE PERFORMANCE USING JP-4 WITH LIQUID OXYGEN AT VARIOUS ALTITUDES

(a) Sea-level performance

Barometric pressure, P_b, lb/sq in. abs	Oxidant-fuel weight ratio, o/f	Total propellant flow, W, lb/sec	Thrust, F, lb	Combustion pressure, P_c, lb/sq in. abs	Ambient pressure, P_o, lb/sq in. abs	Average heat transfer to engine, q_e, Btu/sec sq in.	Average heat transfer to nozzle extension, q_n, Btu/sec sq in.	Characteristic velocity, c^*, ft/sec	Thrust coefficient, C_F	Specific impulse, I, lb-sec/lb	Vacuum thrust coefficient, $C_{F,v}$	Vacuum specific impulse, I_v, lb-sec/lb	Percent of theoretical vacuum specific impulse, I_v, lb-sec/lb	
													Frozen	Equilibrium
Area ratio, 5.49; throat area, 1.145; ejector tube diameter, none; injector number, 3														
14.39	3.04	4.14	1016	603	14.39	2.99	----	5374	1.47	246	1.60	268	93.5	88.6
	2.52	4.08	1011	601		2.57	----	5427	1.47	248	1.60	270	91.9	87.4
	2.89	4.05	997	593		2.94	----	5398	1.47	246	1.60	268	92.8	88.0
	2.59	4.07	1008	601		2.50	----	5441	1.47	248	1.60	270	92.2	87.6
	2.24	3.99	1001	599		2.13	----	5532	1.46	251	1.60	274	92.4	89.0
	1.84	4.08	1015	606		1.72	----	5473	1.46	249	1.60	271	----	----
	2.26	4.06	1013	603		2.15	----	5470	1.47	249	1.60	271	91.5	88.0
	2.65	4.07	1011	600		2.48	----	5457	1.47	249	1.61	271	92.8	88.1
	2.78	4.05	1006	599		2.64	----	5447	1.47	248	1.60	270	93.0	88.2
	2.54	4.00	997	595		2.25	----	5483	1.46	249	1.60	272	92.7	88.1
	2.43	4.04	1003	599		2.21	----	5471	1.46	249	1.60	271	91.9	87.7
Area ratio, 48.39, 49.78; throat area, 1.173, 1.140; ejector tube diameter, none; injector number, 0, 3, 4														
14.19	1.77	[a]4.28	[a]939	614	14.19	----	----	5418	1.30	219	----	---	----	----
14.23	1.71	[a]4.30	[a]939	609	14.23	1.41	0.94	5349	1.31	218	----	---	----	----
14.40	1.80	[a]4.23	[a]938	608	14.40	1.67	1.00	5427	1.32	222	----	---	----	----
14.38	2.59	[a]4.11	[a]915	596	14.38	2.58	1.25	5478	1.31	223	----	---	----	----
	2.39	[a]4.11	[a]919	599		2.21	1.04	5505	1.31	224	----	---	----	----
	2.08	[a]4.16	[a]920	604		2.23	1.12	5486	1.30	221	----	---	----	----
14.34	2.35	[a]3.98	[a]891	601	14.34	2.27	1.00	5543	1.30	223	----	---	----	----
14.36	1.95	4.09	903	615	14.36	1.86	.85	5522	1.29	221	----	---	----	----
14.36	3.19	4.08	882	597	14.36	3.08	1.26	5367	1.30	216	----	---	----	----
14.40	2.41	4.02	881	596	14.40	2.15	1.01	5477	1.30	221	----	---	----	----
	2.03	3.96	881	595		1.80	.92	5547	1.30	224	----	---	----	----
	2.15	4.02	898	607		1.94	.94	5546	1.30	223	----	---	----	----
	2.74	4.01	876	594		2.30	1.07	5433	1.29	218	----	---	----	----
	2.70	3.90	857	580		2.57	1.08	5455	1.30	219	----	---	----	----
	2.01	4.03	889	602		1.88	.88	5516	1.30	222	----	---	----	----
	2.33	3.94	870	586		2.13	.99	5496	1.30	222	----	---	----	----
	1.78	4.09	901	607		1.70	.83	5449	1.30	220	----	---	----	----

(b) Altitude performance

Area ratio, 48.39; throat area, 1.173; ejector tube diameter, 9 in.; injector number, 4														
14.44	2.00	4.16	1196	606	1.55	1.48	0.34	5504	1.68	287	1.81	309	93.3	89.9
	2.45	4.21	1216	609	1.60	2.02	.44	5460	1.70	289	1.83	310	93.4	86.7
	2.80	4.19	1211	607	1.63	2.44	.53	5472	1.70	289	1.83	311	94.9	86.2
	2.62	4.18	1211	610	1.62	2.38	.50	5507	1.69	290	1.82	312	94.3	86.4
	2.28	4.12	1198	604	1.59	1.75	.41	5532	1.69	291	1.82	312	93.5	88.1
	2.27	4.15	1198	604	1.58	2.04	.42	5500	1.69	289	1.82	311	93.0	87.8
	2.00	4.24	1207	611	1.53	1.70	.37	5444	1.68	285	1.80	305	92.3	88.9
	2.06	4.17	1197	604	1.53	1.73	.35	5470	1.69	287	1.81	308	92.9	89.0
	1.56	4.32	1194	612	1.41	1.16	.21	5348	1.66	276	1.78	295	----	----
	1.70	4.36	1218	621	1.50	1.18	.24	5383	1.67	279	1.79	299	----	----
Area ratio, 48.39; throat area, 1.173; ejector tube diameter, $9\frac{5}{8}$ in.; injector number, 4														
14.23	1.62	4.29	1224	608	0.81	1.14	0.23	5355	1.72	286	1.78	296	----	----
	1.64	4.24	1211	601	.69	1.12	.23	5364	1.72	286	1.77	295	----	----
	2.34	4.19	1252	611	.83	1.96	.42	5502	1.75	299	1.81	310	92.8	87.1
	2.37	4.15	1233	604	.83	2.01	.43	5502	1.74	297	1.81	309	92.5	86.5
	2.11	4.14	1232	604	.78	1.60	.35	5506	1.74	297	1.80	308	92.7	88.5
	1.91	4.15	1216	602	.76	1.48	.30	5477	1.72	293	1.78	303	92.3	89.4
	2.70	4.13	1225	596	.83	2.37	.50	5452	1.75	297	1.82	308	93.6	85.3
	2.74	4.20	1249	607	.83	2.56	.53	5452	1.76	297	1.82	308	93.7	85.3
	2.52	4.09	1219	596	.80	2.04	.44	5496	1.75	298	1.81	309	93.1	86.0
	2.14	4.14	1223	601	.78	1.59	.32	5486	1.73	295	1.80	306	91.9	87.6
	2.16	4.13	1227	602	.76	1.71	.36	5508	1.74	297	1.80	308	92.3	87.8
	1.64	4.20	1203	597	.68	1.11	.23	5366	1.72	286	1.77	296	----	----
	2.26	4.07	1208	592	.76	2.15	.44	5496	1.74	297	1.80	307	92.0	86.9
14.19	1.73	4.26	1256	616	.64	----	.28	5459	1.74	295	1.79	303	----	----
	1.80	4.29	1267	620	.65	----	.29	5459	1.74	296	1.79	304	----	----
	1.93	4.21	1256	612	.65	----	.33	5497	1.75	299	1.80	307	93.4	90.3
	2.48	4.11	1247	601	.65	----	.47	5529	1.77	304	1.82	313	94.0	87.2
	3.11	4.14	1230	592	.67	----	.64	5401	1.77	297	1.83	306	94.8	85.7
	1.91	4.18	1249	607	.64	----	.32	5483	1.75	299	1.81	307	93.5	90.6
	2.68	4.15	1243	602	.69	----	.51	5480	1.76	299	1.82	309	93.8	85.6
	2.11	4.14	1249	605	.65	----	.38	5516	1.76	302	1.81	311	93.4	89.2
	2.26	4.13	1250	605	.65	----	.41	5532	1.76	303	1.81	312	93.3	88.1
	1.78	4.26	1264	616	.62	----	.32	5466	1.75	297	1.80	305	----	----
	2.78	4.17	1242	598	.66	----	.52	5425	1.77	298	1.82	307	93.5	85.1
	2.22	4.13	1252	606	.65	----	.42	5534	1.76	303	1.82	312	93.6	88.8
	2.33	4.15	1251	603	.65	----	.45	5492	1.77	302	1.82	311	93.2	87.5
	2.46	3.87	1163	565	.64	----	.46	5505	1.78	300	1.81	310	93.1	86.4

[a]Area of throat was enlarged to 1.173 sq in. from 1.140 sq in., but nozzle exit diameter was constant at 8.50 in.

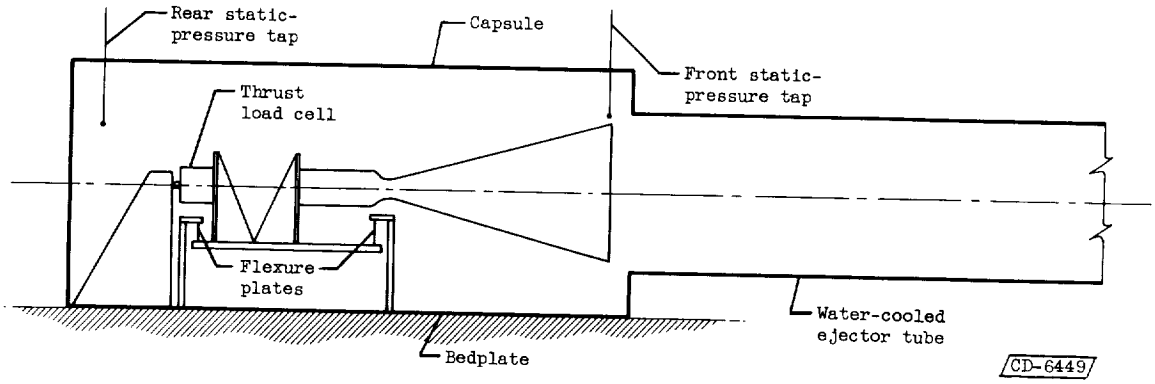

(a) Schematic drawing.

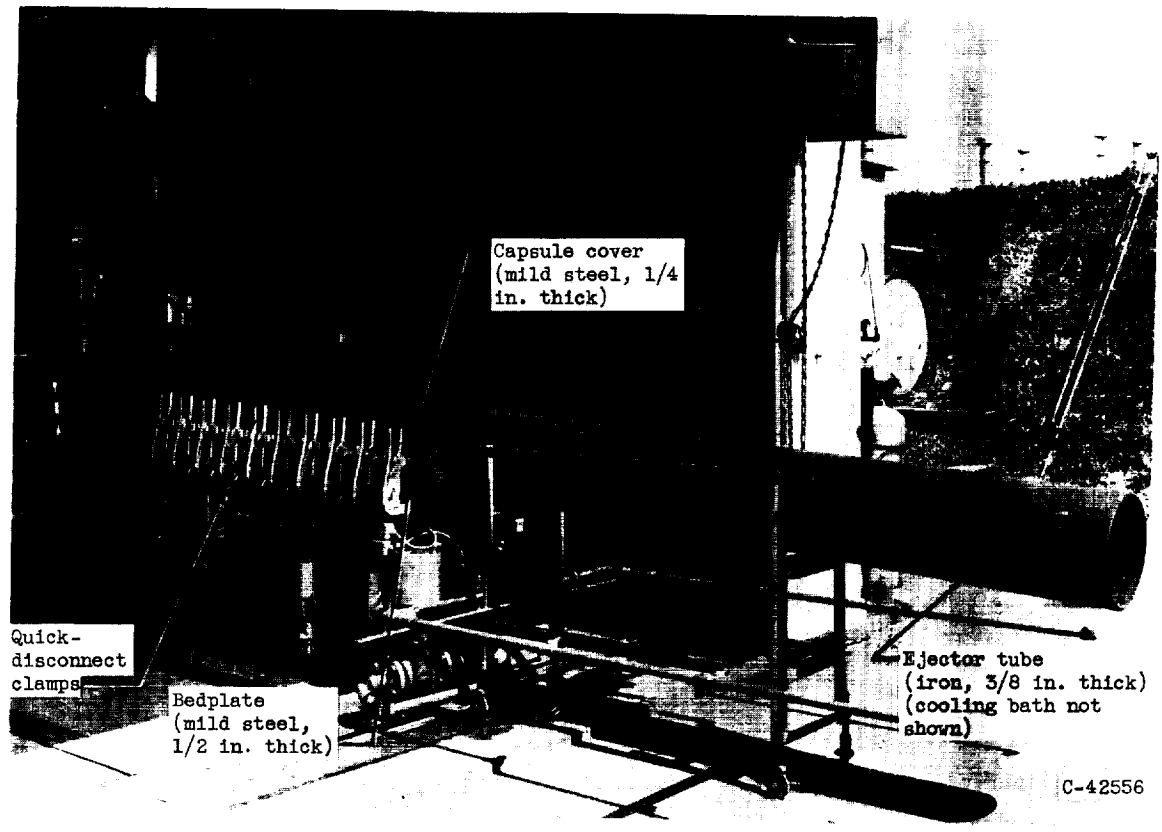

(b) Photograph.

Figure 1. - Rocket test stand and ejector assembly.

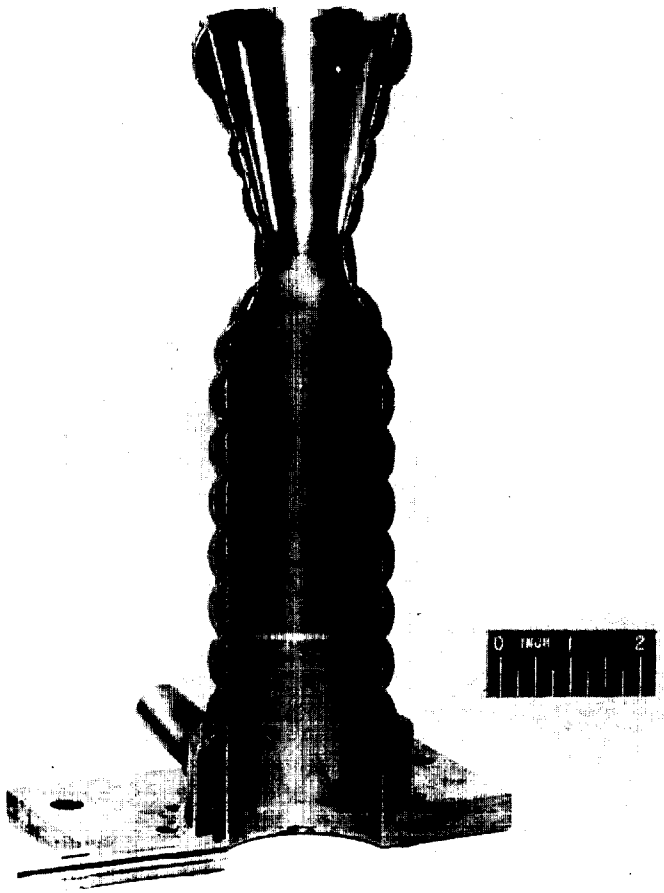

C-36944

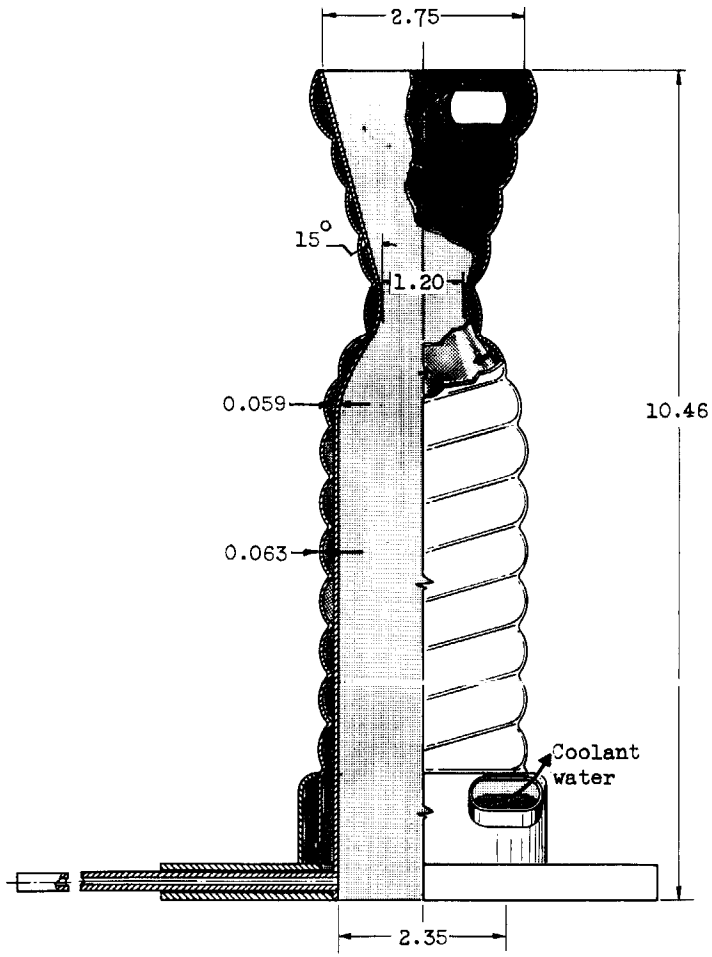

CD-4208

Figure 2. - Cutaway section and diagram of chamber and nozzle of 1000-pound-thrust sea-level rocket engine. (Dimensions in inches.)

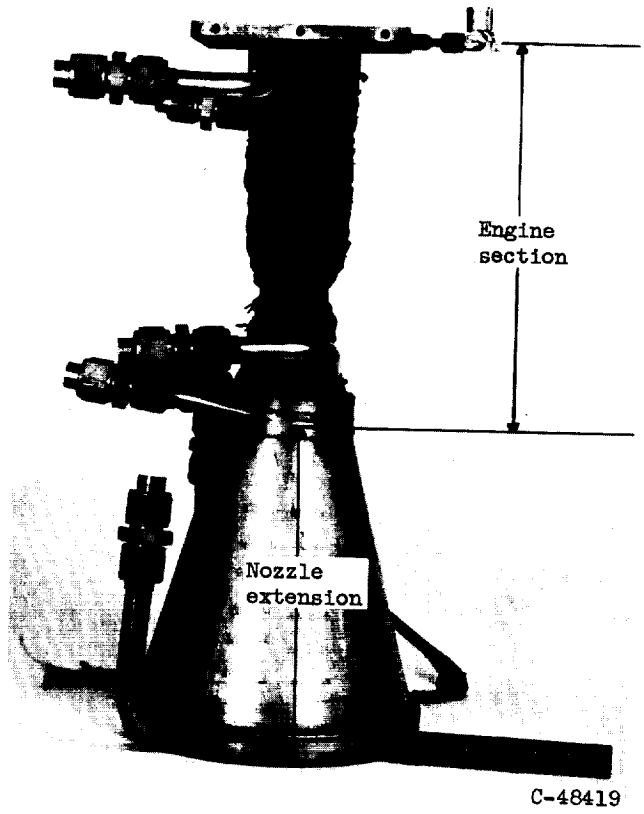

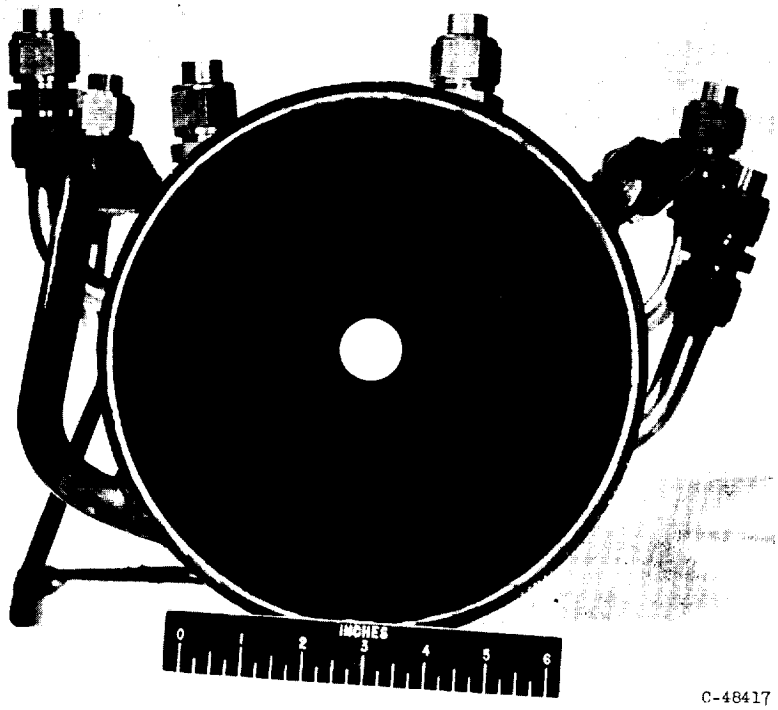

Figure 3. - Large-area-ratio rocket engine (engine section and nozzle extension).

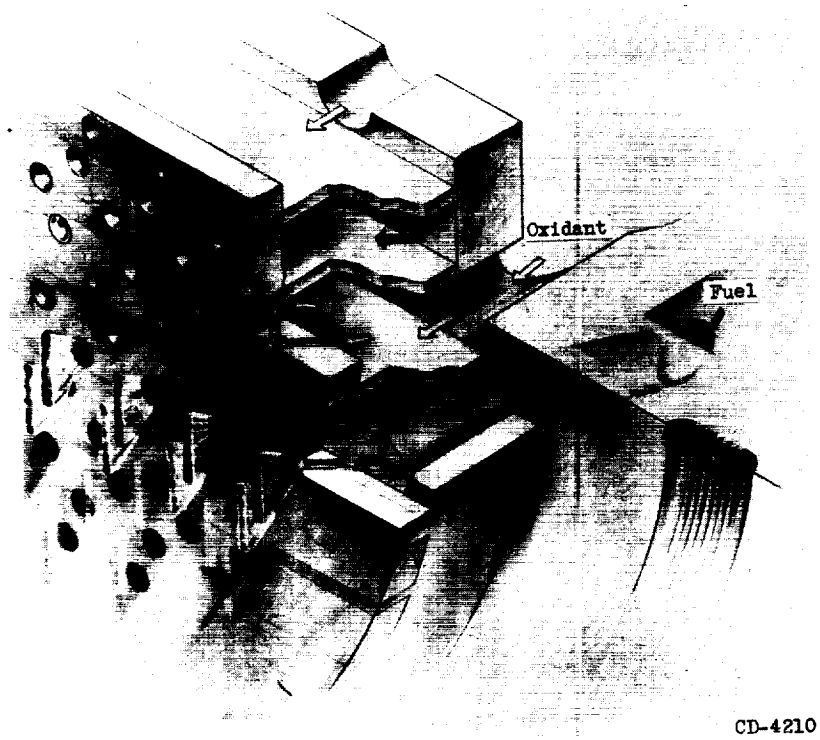

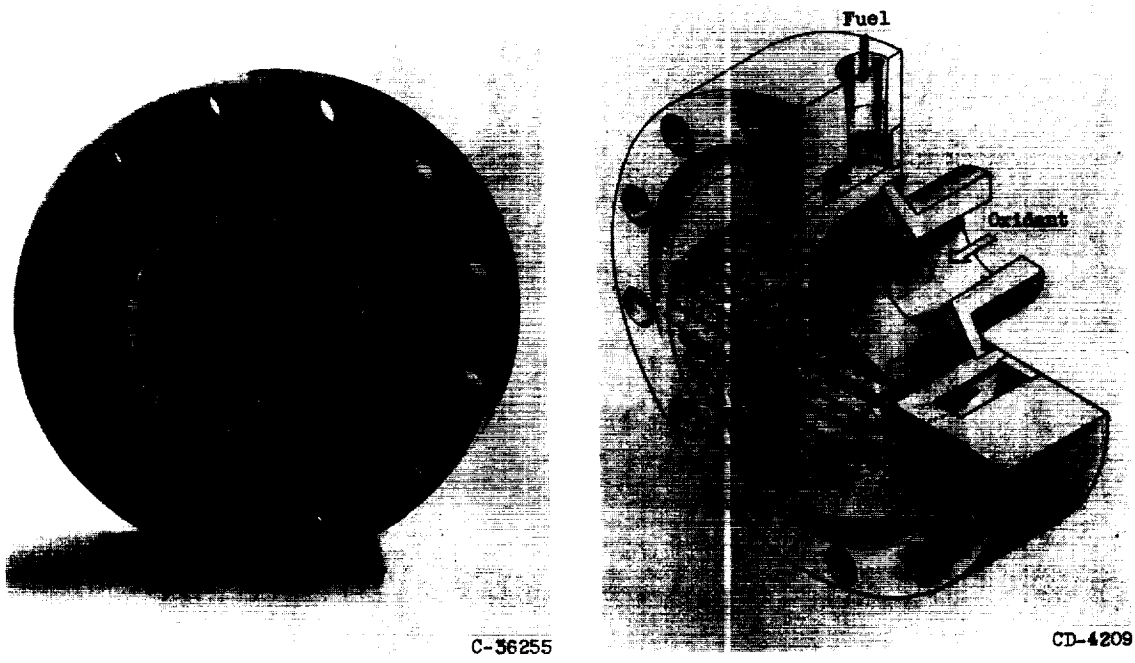

Figure 4. - Like-on-like propellant injector with holes arranged in rows on flat face. (82 pairs of fuel jets, 70 pairs of oxidant jets.)

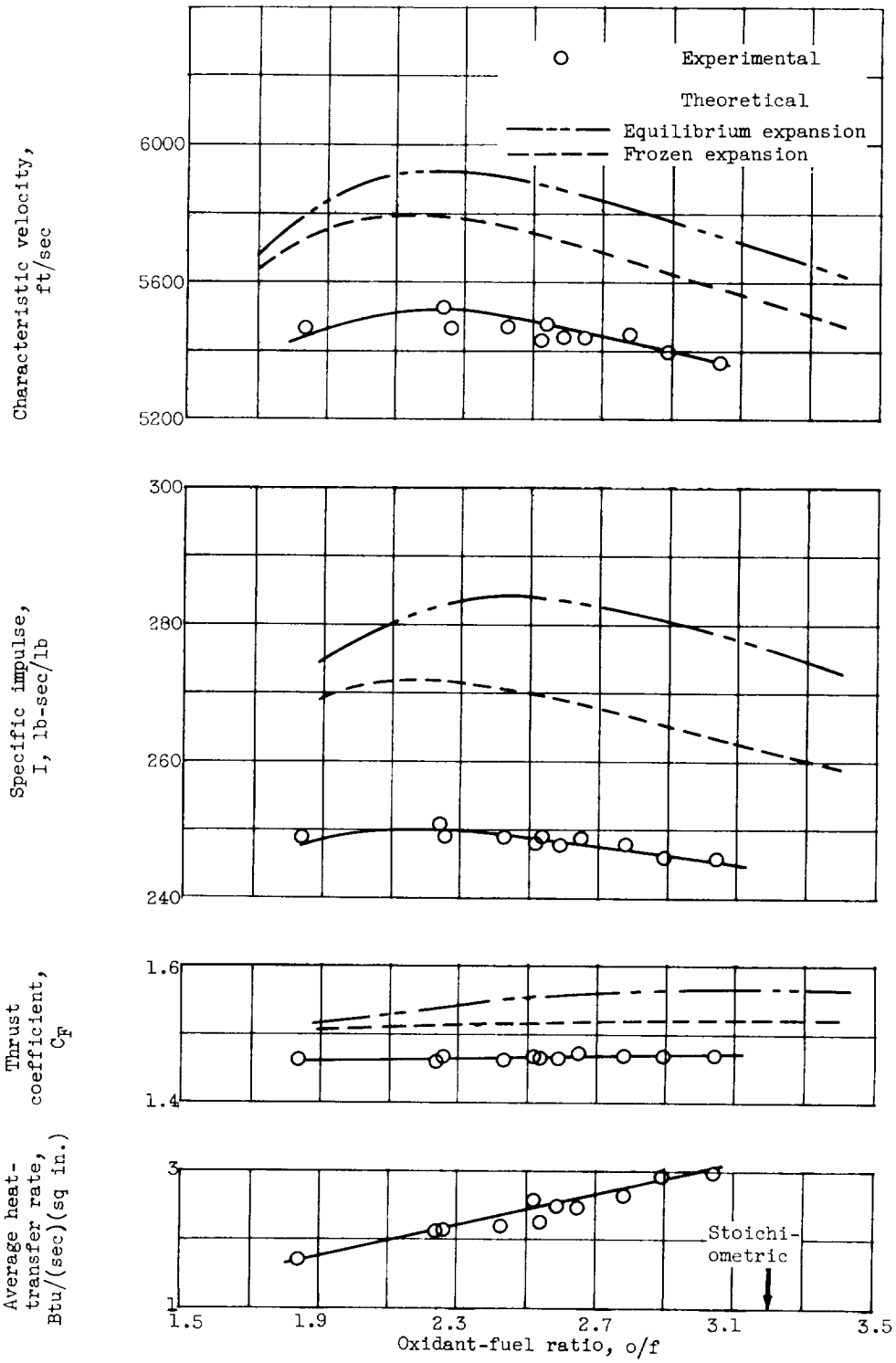

Figure 5. - Experimental and theoretical performance of JP-4 fuel - liquid-oxygen rocket engine having nozzle exit area ratio of 5.49 operating at sea level. Chamber pressure, 600 pounds per square inch absolute.

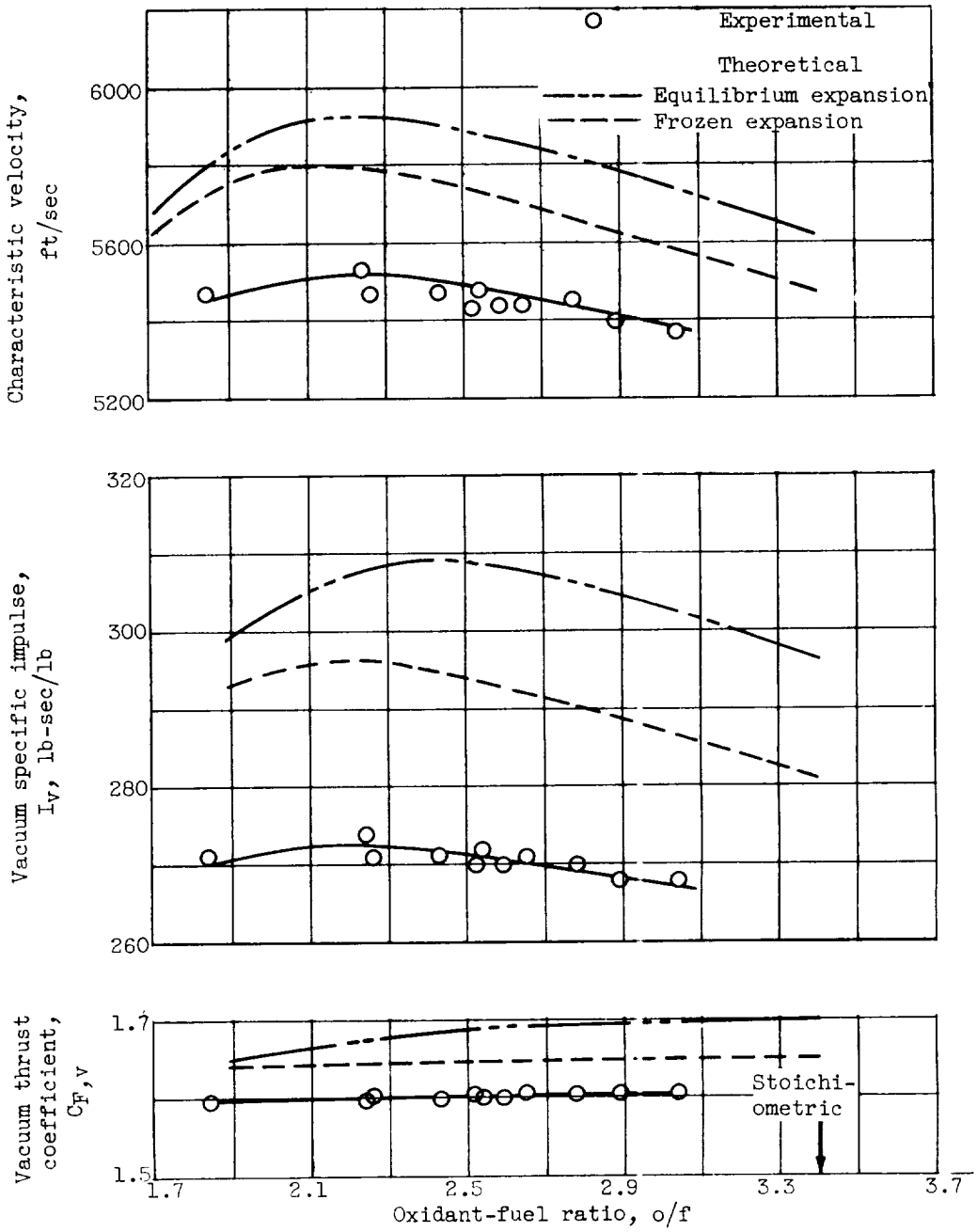

Figure 6. - Experimental and theoretical performance of JP-4 fuel - liquid-oxygen rocket engine having nozzle exit area ratio of 5.49 corrected to vacuum operating conditions. Chamber pressure, 600 pounds per square inch absolute.

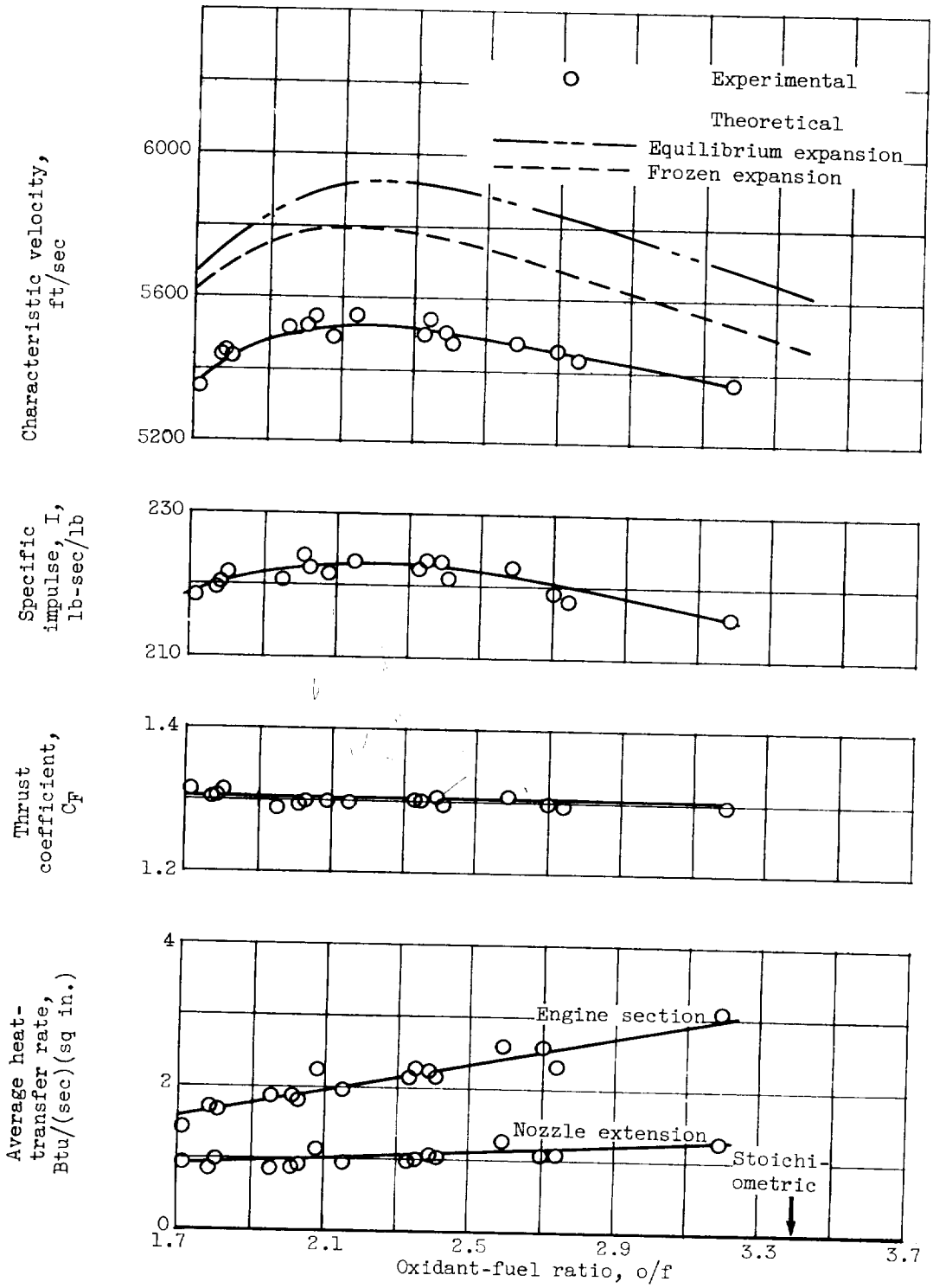

Figure 7. - Experimental and theoretical performance of JP-4 fuel - liquid-oxygen rocket engine having nozzle exit area ratio of 48.39 operating at sea level. Chamber pressure, 600 pounds per square inch absolute.

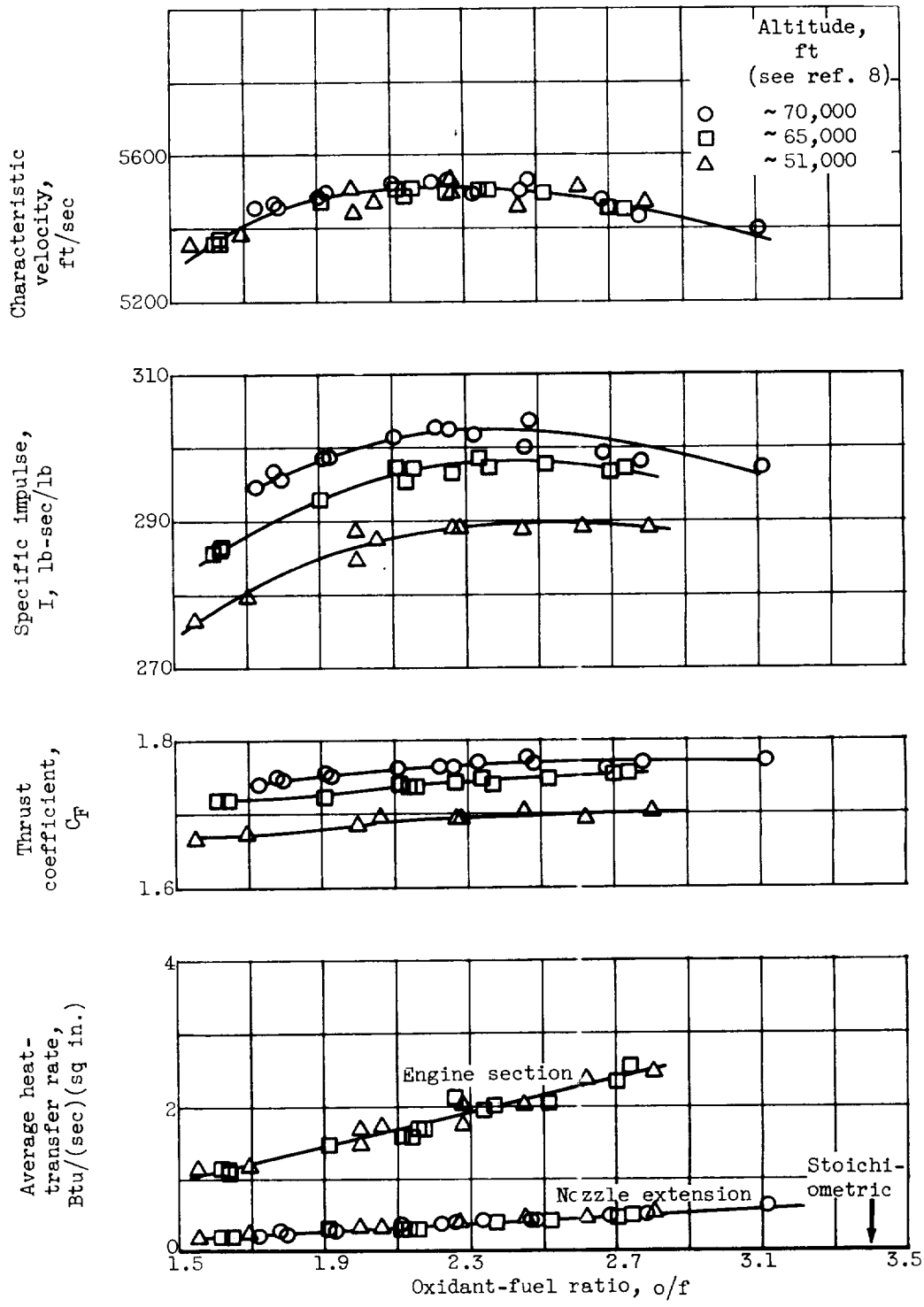

Figure 8. - Experimental performance of JP-4 fuel - liquid-oxygen rocket engine having nozzle exit area ratio of 48.39 operating at three altitude conditions. Chamber pressure, 600 pounds per square inch absolute.

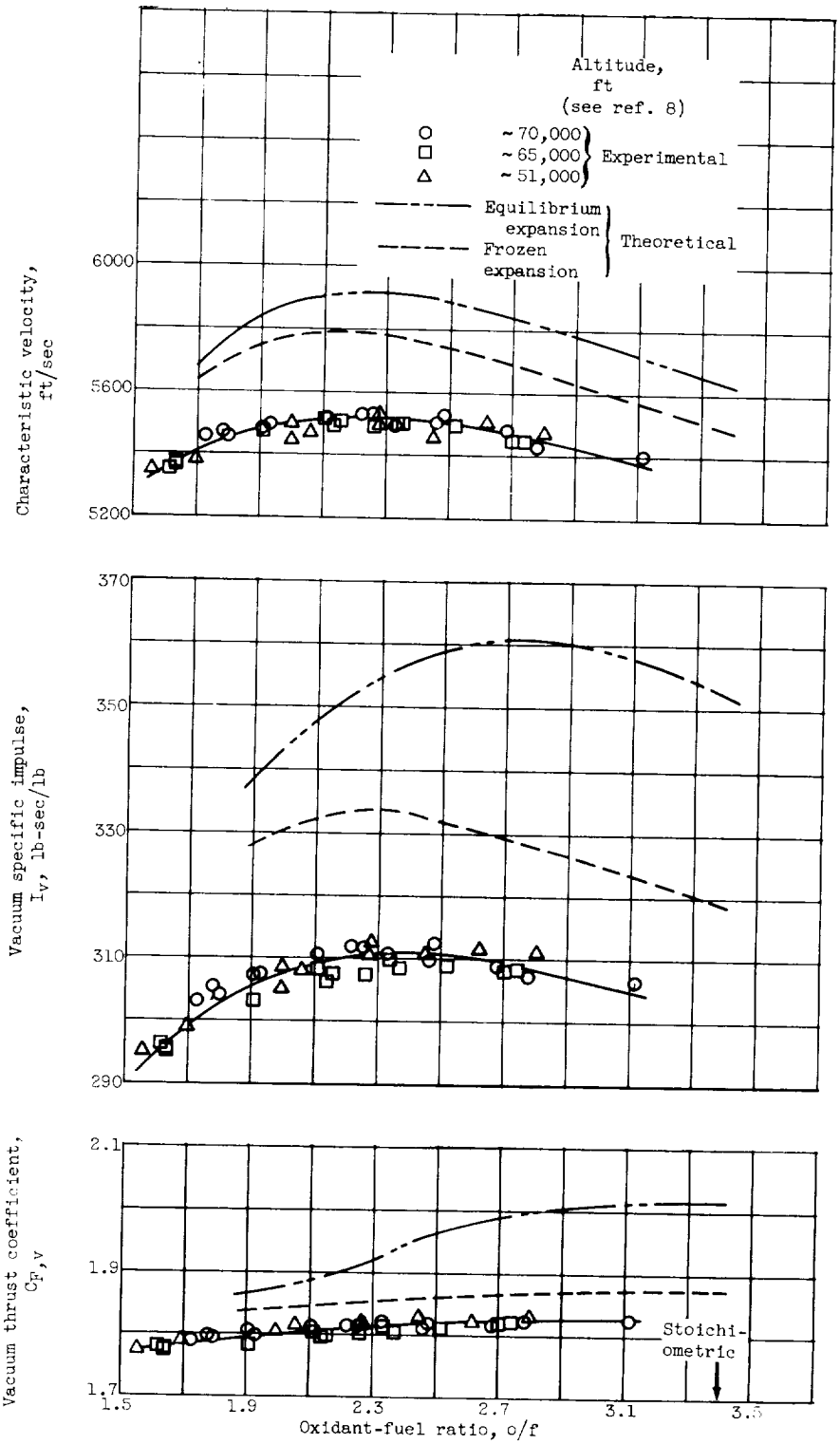

Figure 9. - Experimental and theoretical performance of JP-4 fuel - liquid-oxygen rocket engine having nozzle exit area ratio of 48.39 corrected to vacuum operating conditions. Chamber pressure, 600 pounds per square inch absolute.

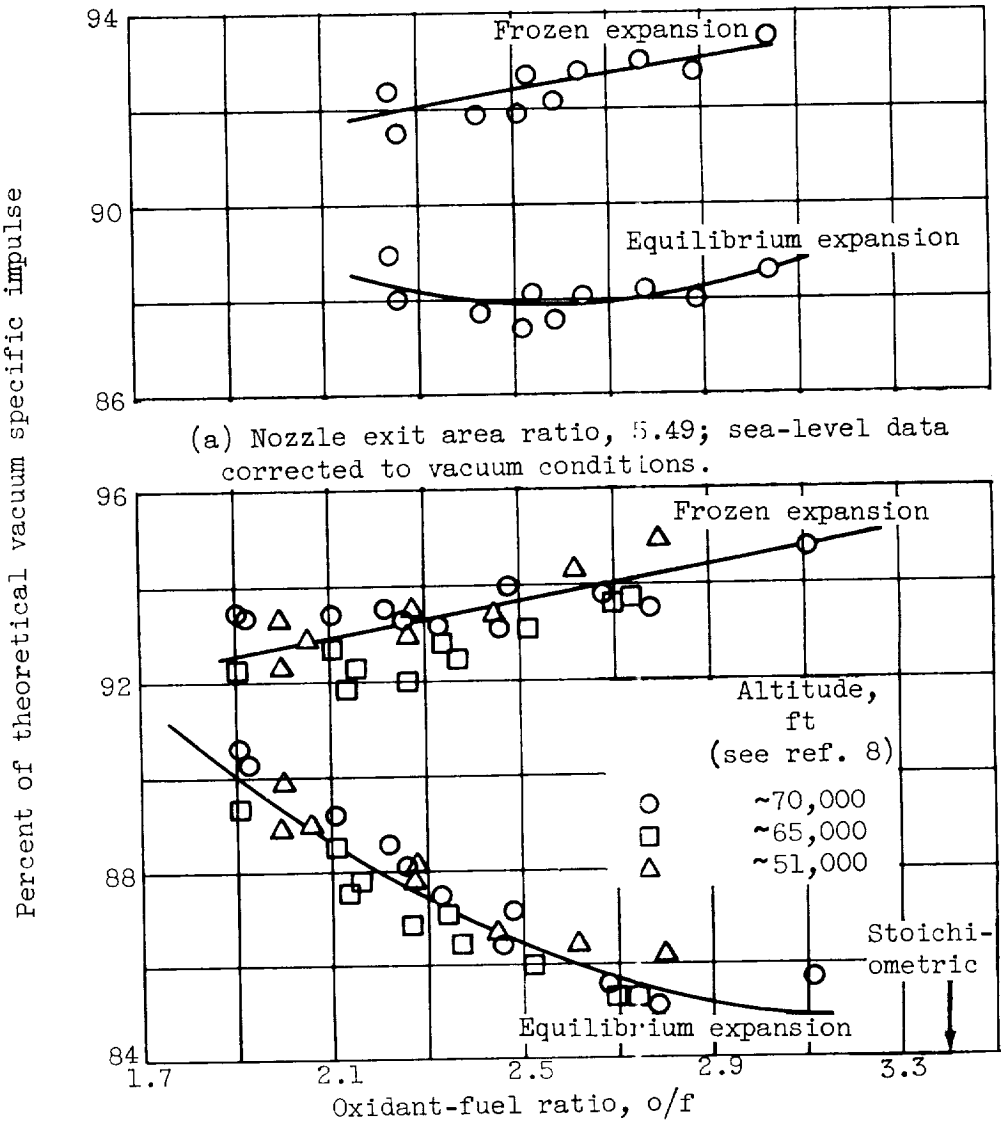

(a) Nozzle exit area ratio, 5.49; sea-level data corrected to vacuum conditions.

(b) Nozzle exit area ratio, 48.39; altitude data corrected to vacuum conditions.

Figure 10. - Percent of theoretical vacuum specific impulse for JP-4 fuel - liquid-oxygen rocket engine having nozzle exit area ratio of 5.49 or 48.39. Chamber pressure, 600 pounds per square inch absolute.

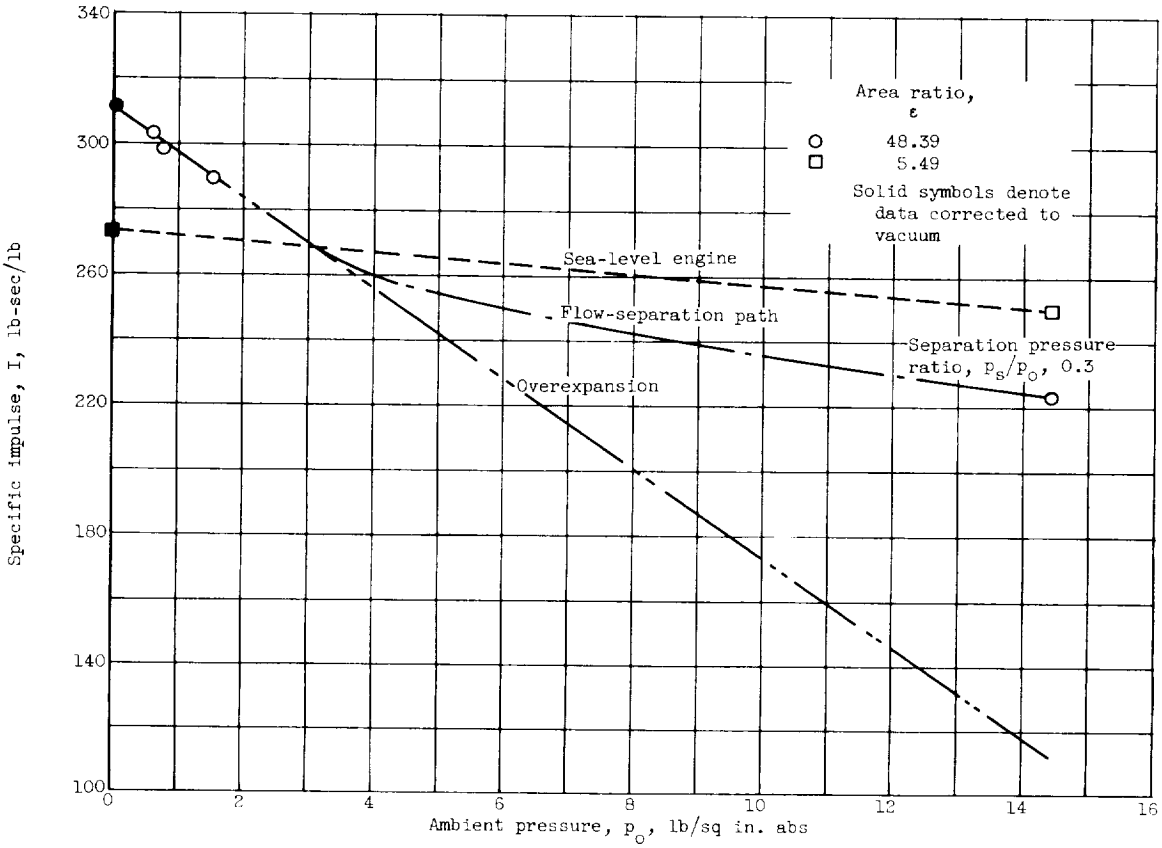

Figure 11. - Experimental specific impulse for JP-4 fuel - liquid-oxygen rocket engine having nozzle exit area ratio of 5.49 or 48.39 operating at various ambient pressures. Chamber pressure, 600 pounds per square inch absolute; oxidant-fuel ratio, 2.30.